

Two distinct excitable responses for a laser with a saturable absorber

Thomas Erneux

Université Libre de Bruxelles, Optique Nonlinéaire Théorique, Campus Plaine, CP 231, 1050 Bruxelles, Belgium

Sylvain Barbay

Centre de Nanosciences et de Nanotechnologies, CNRS, Université Paris-Sud, Université Paris-Saclay, site de Marcoussis, 91460 Marcoussis, France

(Received 16 October 2017; published 19 June 2018)

Excitable lasers with saturable absorbers are currently investigated as potential candidates for low level spike processing tasks in integrated optical platforms. Following a small perturbation of a stable equilibrium, a single and intense laser pulse can be generated before returning to rest. Motivated by recent experiments [Selmi *et al.*, *Phys. Rev. E* **94**, 042219 (2016)], we consider the rate equations for a laser containing a saturable absorber (LSA) and analyze the effects of different initial perturbations. With its three steady states and following Hodgkin classification, the LSA is a Type I excitable system. By contrast to perturbations on the intensity leading to the same intensity pulse, perturbations on the gain generate pulses of different amplitudes. We explain these distinct behaviors by analyzing the slow-fast dynamics of the laser in each case. We first consider a two-variable LSA model for which the conditions of excitability can be explored in the phase plane in a transparent manner. We then concentrate on the full three variable LSA equations and analyze its solutions near a degenerate steady bifurcation point. This analysis generalizes previous results [Dubbeldam *et al.*, *Phys. Rev. E* **60**, 6580 (1999)] for unequal carrier density rates. Last, we discuss a fundamental difference between neuron and laser models.

DOI: [10.1103/PhysRevE.97.062214](https://doi.org/10.1103/PhysRevE.97.062214)**I. INTRODUCTION**

Excitable systems play an important role in biology and medicine. Phenomena such as the transmission of impulses between neurons, the cardiac arrhythmia, the aggregation of amoebas, all derive from the activity of excitable media [1–3]. Common to all these excitable systems is the existence of a stable equilibrium and an excited or firing regime. For weak stimuli, the system returns more or less directly to rest. For stronger stimuli, it makes a large detour, that is, emits a spike. In the case of neuronal firing, two main types of excitable responses have been classified by Hodgkin in the 1940s [4]. Type I axons have sharp threshold and can have long latency to firing. Type I models are characterized by a set of three fixed points, a stable one, a saddle, and an unstable one. Type II have variable thresholds and short latency. Type II models exhibit only one stable fixed point.

Excitable responses were also predicted and observed in a large variety of optical systems, ranging from nonlinear cavities with temperature dependent absorption [5] to lasers with a saturable absorber (LSA) [6–10] or subject to either optical feedback [11,12] or optical injection [13–15]. The recent interest in spiking neural networks (SNN) using photonic platforms has revived research activities on excitable lasers [16–20]. The challenge is to produce an optical network where each node has the response characteristics of a neuron and is capable to process information at high speeds. In [17], a nanoscale resonant tunneling diode behaves like an excitable biological oscillator and drives an on-chip laser diode [21]. Recently, it was demonstrated that micropillar semiconductor lasers with integrated saturable absorbers may generate

excitable responses in time intervals of the order of 200 ps. Threshold conditions and refractory periods were analyzed experimentally and numerically in [22]. Numerical simulations were realized by considering the three rate equations for a LSA that relate the density of photons (intensity) to the carrier densities (electrons) in the active and passive media. Particular attention was devoted to the time needed for the emergence of an active spike [23] (spike latency). With its three steady states, the LSA is a Type I excitable system but, as we shall demonstrate, the response of the laser may depend on the initial perturbation.

In [23], excitable pulses were initiated by either perturbing the laser intensity (coherent perturbation) or by perturbing the carrier density (incoherent perturbation) [23]. Practically, short optical pulses were injected into the laser with different wavelengths. If the wavelength is close to the cavity resonance wavelength, the perturbation was called “coherent” On the other hand, if the wavelength of the stimulation is quite different from the cavity resonance wavelength and only affects the carrier density, the perturbation was called “incoherent” and its effect is described by a change of the initial gain value. Figure 1 shows experimental time traces resulting from these two types of perturbations. From left to right, we represent the laser intensity after a below, a slightly above, and a well above critical perturbation. We note that the maximum intensity of the pulse increases with the initial perturbation in the case of an incoherent perturbation [Fig. 1(a)] while it remains quasi-constant in the case of a coherent perturbation [Fig. 1(b)]. The effect of an incoherent perturbation is not observed for Type I neurons and need to be clarified. To this end, we first consider a two-variable LSA model for which conditions for

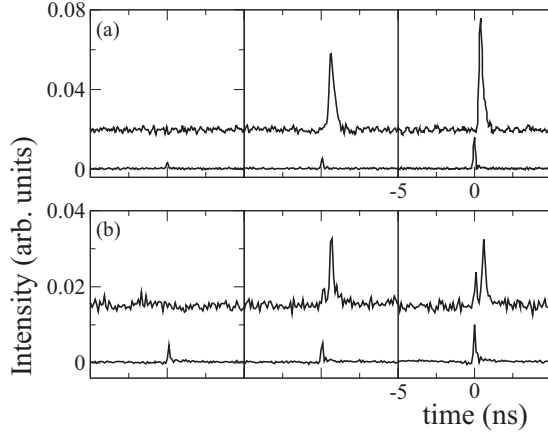


FIG. 1. Experimental temporal traces following an incoherent (a) or a coherent (b) perturbation. For each case, we show the laser response (top) and the initial perturbation (bottom). From left to right, the initial perturbation is below, slightly above, and well above the critical perturbation for excitability. The response signal is vertically shifted for clarity. In both figures, we note that the laser response follows the initial perturbation after a delay.

excitability can be discussed in phase-space in a transparent manner.

The solution of the three laser equations exhibits different amplitude and time scales which motivate the application of asymptotic methods. Dubbeldam *et al.* [6] consider the case of equal relaxation rates of the gain and absorber and examined the effects of initial intensity perturbations. They obtained analytical approximations for the excitability threshold and the delay between input and output pulses. Here, we consider unequal relaxation rates for the gain and absorber and propose a systematic perturbation analysis of the LSA equations. This generalization is physically motivated by the fact that there are usually different recombination rates in the gain and in the absorber regions because of either different carrier densities or materials.

The organization of the paper is as follows. In Sec. II, we formulate the laser rate equations and specify the initial conditions for a coherent and an incoherent perturbation. In Sec. III, we consider a two variable reduction of the LSA equations and analyze the conditions for an excitable pulse for both coherent and incoherent perturbations. In Sec. IV, we then consider the three variable LSA equations and analyze the pulse solutions near a degenerate bifurcation point. Finally, we contrast neuron and LSA slow fast responses in Sec. V by showing that the laser pulse is of Lotka-Volterra type rather than van der Pol type.

II. FORMULATION

In a LSA, two spatially separated sections are placed in the laser cavity. The role of the two sections is quite different: one of them is pumped so as to have a positive population inversion (active or amplifying medium), the other one is left with a negative population inversion (passive or absorbing medium). As these two media are in general different, they saturate at different power levels. The most interesting case

corresponds to the situation where the absorber saturates more easily than the active medium, introducing nonlinear losses inside the cavity. The output of many LSAs is well described as the solution of three rate equations for the field in the laser cavity and the population inversions (or carrier densities) in the active and passive cells [25]. Here, we follow the formulation successfully used in [22,23] to simulate the experiments given by

$$I' = (G - Q - 1)I, \quad (1)$$

$$G' = b_1[\mu_1 - G(1 + I)], \quad (2)$$

$$Q' = b_2[\mu_2 - Q(1 + sI)]. \quad (3)$$

In these equations, I is the laser intra-cavity intensity. G and Q are the scaled excess carrier densities with respect to transparency in the gain and in the saturable region (SA), respectively. μ_1 denotes the gain generated through pumping, μ_2 is the non-saturable loss, and s is the saturation parameter. Prime means differentiation with respect to time t rescaled to the cavity lifetime. $b_{1,2}$ are the rescaled recombination rates of carriers in the gain and SA regions, respectively. They are typically $O(10^{-3})$ small. Note that s depends on b_1 and b_2 [24]. Throughout this paper, we consider the following values of b_1 , b_2 , μ_2 , and s appropriate for the laser used in the experiments [22,23]

$$b_1 = 10^{-3}, \quad b_2 = 2 \times 10^{-3}, \quad \mu_2 = 2, \quad \text{and} \quad s = 10. \quad (4)$$

Our control parameter is the pump parameter μ_1 . Its value as well as the initial conditions will be specified later. In all our simulations, we have added the constant $c = 10^{-35}$ in the right-hand side of Eq. (1) in order to avoid extremely low values of the intensity. This is physically justified by the presence of spontaneous emission in the laser cavity.

Before we analyze Eqs. (1)–(3), we need to specify some of the bifurcation properties of the steady states. From the linearized equations, we obtain the following growth rates for the stability of the zero intensity steady state $(I, G, Q) = (0, \mu_1, \mu_2)$:

$$\lambda_1 = \mu_1 - \mu_{1th}, \quad \lambda_2 = -b_1, \quad \lambda_3 = -b_2, \quad (5)$$

where $\mu_{1th} \equiv 1 + \mu_2$ is called the laser threshold. The zero intensity steady state is stable if

$$\mu_1 < \mu_{1th} \quad (6)$$

and unstable otherwise. Similarly, we may analyze the stability of the non-zero intensity steady state. The latter emerges from the steady bifurcation point $\mu_1 = \mu_{1th}$. The bifurcation is subcritical if

$$\mu_{1th} - s\mu_2 < 0 \quad (7)$$

and leads to a branch of unstable steady states. Close to its bifurcation point, the steady state intensity is given by

$$I_s = \frac{\mu_1 - \mu_{1th}}{\mu_{1th} - s\mu_2}, \quad |\mu_1 - \mu_{1th}| \rightarrow 0. \quad (8)$$

The branch of unstable steady states grows in intensity as μ_1 further deviate from μ_{1th} and folds back at $\mu_1 = \mu_{1L} < \mu_{1th}$. It then continues to grow in intensity and finally stabilizes

through a Hopf bifurcation point at $\mu_{1H} \gg \mu_{1th}$ [25]. The condition (7) is verified for the parameters listed in Eq. (4).

The inequality (6) restricts the values of μ_1 for a stable zero intensity steady state. With $\mu_1 < \mu_{1th}$ fixed, we wonder if a small perturbation may or may not lead to an excitable laser pulse. A coherent perturbation is described as an initial perturbation of a stable zero intensity steady state. The initial conditions then are

$$I(0) = I_p, G(0) = \mu_1, \quad \text{and} \quad Q(0) = \mu_2. \quad (9)$$

This problem was previously considered in [6] in the case of equal carrier recombination rates ($b_1 = b_2$). The authors developed approximations that do not generalize easily in the case $b_1 \neq b_2$. Here, we propose an alternative and more systematic analytical approach that applies both to coherent and incoherent perturbations.

The case of an incoherent perturbation considers perturbations on the gain and is described by the initial conditions

$$I(0) = I_0, G(0) = G_p \neq \mu_1, \quad \text{and} \quad Q(0) = \mu_2. \quad (10)$$

III. TWO VARIABLE LSA EQUATIONS

In order to clearly explain the two types of excitable responses observed experimentally, we examine the case of a fast absorber ($b_2 \gg b_1$). In this case, we may eliminate the carrier for the absorber by a quasi-steady state approximation and obtain

$$I' = \left(G - 1 - \frac{\mu_2}{1 + sI} \right) I, \quad (11)$$

$$G' = b_1[\mu_1 - G(1 + I)]. \quad (12)$$

A. Coherent perturbation

Equations (11) and (12) allow us to analyze trajectories in the phase-plane (G, I) without any assumptions on the parameter values. The I and G nullclines are lines satisfying Eq. (11) with $I' = 0$ and Eq. (12) with $G' = 0$, respectively. They are given by

$$(1a) I = 0 \quad \text{and} \quad (1b) G = 1 + \frac{\mu_2}{1 + sI} \quad (G \leq 1 + \mu_2), \quad (13)$$

$$(2) G = \frac{\mu_1}{1 + I} \quad (G \leq \mu_1), \quad (14)$$

and are shown in Fig. 2. Successful excitable trajectories are possible if the initial perturbation surpasses the stable manifold of the saddle. From the equation for the trajectories $G = G(I)$,

$$\frac{dG}{dI} = \frac{b_1[\mu_1 - G(1 + I)]}{\left(G - 1 - \frac{\mu_2}{1 + sI} \right) I}, \quad (15)$$

we deduce that the stable manifold is either the straight line $I = 0$ or $G = G_s(I, b_1)$ given by

$$G_s = 1 + \frac{\mu_2}{1 + sI} + O(b_1) \quad (b_1 \rightarrow 0) \quad (16)$$

which is close to the nullcline (1b). On the other hand, the fast unstable manifold $G = G_u(I, b_1)$ verifies $dG/dI = 0$ as $b_1 \rightarrow 0$, i.e., G_u equals its steady state value at the saddle. The two manifolds are shown by broken lines in Fig. 2.

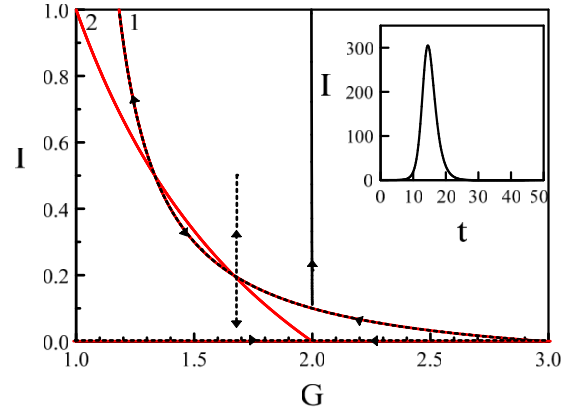


FIG. 2. Coherent perturbation. The curves labeled by 1 and 2 are the nullclines (13) and (14). Their intersections are fixed points namely, the stable zero intensity steady state $(G, I) = (2.0, 0)$, the unstable saddle $(G, I) = (1.7, 0.2)$, and the unstable focus $(G, I) = (1.3, 0.5)$. Parameter values are $\mu_2 = 2$, $s = 10$, $b_1 = 10^{-3}$, $\mu_1 = 2$, $G(0) = \mu_1$, and $I(0) = 0.11$ which is larger than the critical perturbation $I_{pc} = 0.10$. The inset shows the intensity I as a function of time t .

For a coherent perturbation, we start with the laser resting at its stable zero intensity steady state $(G, I) = (\mu_1, 0)$ and consider the initial conditions:

$$I(0) = I_p \quad \text{and} \quad G(0) = \mu_1. \quad (17)$$

Figure 2 represents the early stage of a successful excitable pulse in the phase-plane (G, I). The pulse is possible provided I_p surpasses the stable manifold (separatrix) (16). From Eq. (16) with $G_s = \mu_1$, we determine the critical perturbation I_{pc} . The condition for a successful intensity pulse then is

$$I_p > I_{pc} \equiv \frac{\mu_2 + 1 - \mu_1}{(\mu_1 - 1)s} \quad (1 < \mu_1 < \mu_{1th}). \quad (18)$$

As soon the pulse is initiated, the intensity quickly moves to high values. Assuming $I = O(b_1^{-1})$, Eqs. (11) and (12) reduce to

$$I' = (G - 1)I, \quad (19)$$

$$G' = -b_1GI \quad (b_1 \rightarrow 0), \quad (20)$$

in first approximation. Equations (19) and (20) can be integrated in the phase plane because the first-order equation for dI/dG is separable [25]. We find

$$I - I(0) = b_1^{-1}(-G + G(0)) + \ln(G/G(0)). \quad (21)$$

From Eq. (18), we note that the maximum intensity appears at $G = 1$. Since $G(0) = \mu_1$ and $I(0) = I_p \ll I$, Eq. (21) leads to ([25] (8.38) p. 190)

$$I_m = b_1^{-1}[\mu_1 - 1 - \ln(\mu_1)]. \quad (22)$$

μ_1 is fixed and I_p does not appear in Eq. (22). Therefore, the amplitude of the excitable pulse doesn't depend on its initial stimulus.

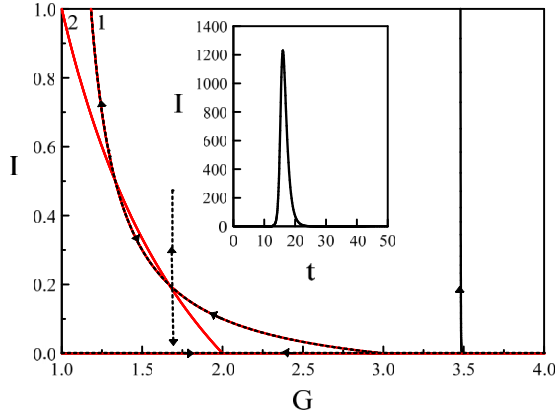


FIG. 3. Perturbation on the gain. The curves labeled by 1 and 2 refer to the two nullclines defined by Eqs. (13) and (14). The parameter values are $\mu_2 = 2$, $s = 10$, $b_1 = 10^{-3}$, $\mu_1 = 2$, $I_0 = 0.2$, and $G_p = 3.5$. The inset shows the intensity I as a function of t .

B. Incoherent perturbation

An incoherent perturbation is defined as a perturbation on the gain. The initial conditions now are

$$I(0) = I_0 \text{ and } G(0) = G_p, \quad (23)$$

where $I_0 \neq 0$ (if $I_0 = 0$, the trajectory follows the line $I = 0$ until $G = \mu_1$). Analyzing the trajectories in the phase-plane (see Fig. 3) now provides the following conditions for an excitable pulse:

$$\mu_1 < \mu_{1th} : G_p > G_{pc} = 1 + \frac{\mu_2}{1 + sI_0} + O(b_1), \quad (24)$$

$$\mu_1 > \mu_{1th} : G_p \text{ arbitrary}, \quad (25)$$

where G_{pc} is the stable manifold (16) evaluated at $I = I_0$. The maximum intensity again appears at $G = 1$. Using Eq. (21) with $G(0) = G_p$ and $I(0) = I_0 \ll b_1^{-1}$, we obtain

$$I_m = b_1^{-1}[-(1 - G_p) + \ln(1/G_p)]. \quad (26)$$

By contrast to the case of a coherent perturbation, increasing the perturbation G_p leads to an increase of the maximum intensity. Physically, the gain perturbation changes the carrier density and hence the gain of the laser itself, leading to an increase of the response pulse amplitude.

IV. CLOSE TO THE LSA BIFURCATION POINT

We now wish to analyze the full LSA equations (1)–(3). To this end, we apply bifurcation techniques and consider $|\mu_1 - \mu_{1th}|$ and $b_{1,2}$ as small parameters. Specifically, we analyze the singular limit $b_{1,2} \rightarrow 0$ and $\mu_1 - \mu_{1th} \rightarrow 0^-$ of Eqs. (1)–(3). The limit is singular because all three eigenvalues in Eq. (5) are zero if $b_{1,2} = \mu_1 - \mu_{1th} = 0$. The steady bifurcation point at $\mu_1 = \mu_{1th}$ corresponds to a triple zero eigenvalue.

A. Coherent perturbation

We first analyze the case of a coherent perturbation by considering the initial conditions (9). Figure 4 illustrates the emergence of an excitable pulse for different perturbations I_p . We note in Fig. 4(a) that the amplitude of the intensity remains

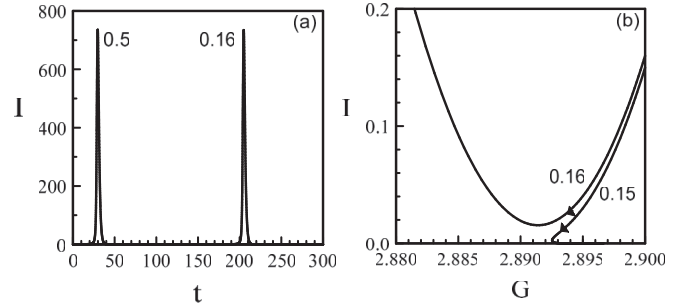


FIG. 4. Excitable pulses initiated by a coherent perturbation. The critical perturbation for excitability verifies the inequality $0.15 < I_{pc} < 0.16$. (a) Two intensity pulses are initiated by a perturbation I_p close and far from I_{pc} . (b) Low intensity phase-plane (G, I) showing trajectories for a below and an above critical perturbation. The values of the parameters are listed in Eq. (4) and $\mu_1 = 2.9$.

quasi-constant if we increase I_p . This is consistent with the experimental observations [see Fig. 1(b)]. Only the spiking time decreases with I_p . Figure 4(b) shows two trajectories for two different values of I_p . Only one leads to a successful excitable pulse ($I_p = 0.16$). The critical perturbation I_{pc} ($0.15 < I_{pc} < 0.16$) has an analytical approximation derived below and given by Eq. (42). Using the parameters listed in Eq. (4) and $\mu_1 = 2.9$, we find $I_{pc} \simeq 0.14$.

To remove the singularity appearing when $b_{1,2} \rightarrow 0$, we reformulate Eqs. (1)–(3) in a form where b_1 and b_2 are no longer multiplying the right-hand sides of Eqs. (2) and (3). This is realized by a particular scaling between $b_{1,2}$ and the deviations of G and Q from their steady state values $G = \mu_1$ and $Q = \mu_2$, respectively. This scaling is inspired by the singularity appearing in the equations for a single mode laser and the method used to remove it (see [25], p. 119). Specifically, we first introduce a small parameter ε defined by

$$\varepsilon \equiv \sqrt{b_1} \quad (27)$$

and assume

$$b_2 = \varepsilon^2 b_{21} \quad \text{and} \quad \mu_1 = \mu_{1th} + \varepsilon\alpha, \quad (28)$$

where both b_{21} and $\alpha < 0$ are $O(1)$ quantities. Because $G(0)$ and $Q(0)$ are equal to their steady state values, we introduce the deviations εg and εq defined by

$$\varepsilon g \equiv G - \mu_1 \quad \text{and} \quad \varepsilon q \equiv Q - \mu_2, \quad (29)$$

where both g and q are $O(1)$ functions of time. After inserting Eqs. (27) and (29) into Eqs. (1)–(3), we obtain

$$I' = (\alpha + g - q)I, \quad (30)$$

$$g' = -\varepsilon g - (\mu_{1th} + \varepsilon\alpha + \varepsilon g)I, \quad (31)$$

$$q' = b_{21}[-\varepsilon q - (\mu_2 + \varepsilon q)sI], \quad (32)$$

where prime now means differentiation with respect to time $T \equiv \varepsilon t$. The limit of small recombination rates $b_{1,2}$ now correspond to the limit $\varepsilon \rightarrow 0$ which is no longer singular. Setting $\varepsilon = 0$ in Eqs. (30)–(32) leads to the following reduced

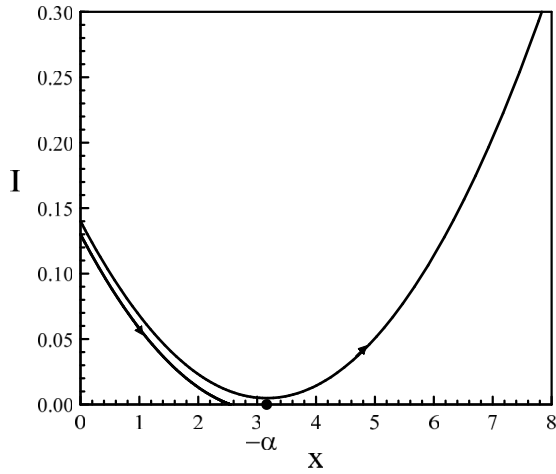


FIG. 5. Two trajectories initiated by slightly different perturbations I_p are shown in the (x, I) phase plane. They have been obtained by solving numerically Eqs. (37) and (38) with $I_p = 0.13 < I_{pc} \simeq 0.135$ and $I_p = 0.14 > I_{pc}$. The values of the parameters are listed in Eq. (4) and $\mu_1 = 2.9$.

problem for I , g , and q :

$$I' = (\alpha + g - q)I, \quad (33)$$

$$g' = -\mu_{1th}I, \quad (34)$$

$$q' = -b_{21}\mu_{2s}I. \quad (35)$$

Next introducing

$$x \equiv g - q, \quad (36)$$

we obtain from Eqs. (33)–(35) two coupled equations for I and x given by

$$I' = (\alpha + x)I, \quad (37)$$

$$x' = (b_{21}\mu_{2s} - \mu_{1th})I. \quad (38)$$

From Eqs. (9) and (29), we note that $g(0) = q(0) = 0$. The initial conditions for I and x then are

$$I(0) = I_p \text{ and } x(0) = 0. \quad (39)$$

Dividing Eqs. (37) and (38) side by side, we obtain a first-order equation for $I = I(x)$ which can be integrated. We find

$$I = I_p + \frac{1}{2(b_{21}\mu_{2s} - \mu_{1th})}((\alpha + x)^2 - \alpha^2). \quad (40)$$

Figure 5 shows two trajectories in the phase plane (x, I) for two distinct values of I_p . A successful excitable pulse is possible if $I_p > I_{pc}$. I_{pc} is defined as the initial condition that leads to the saddle $(x, I) = (-\alpha, 0)$. Using Eq. (40), we obtain

$$I_{pc} = \frac{\alpha^2}{2(b_{21}\mu_{2s} - \mu_{1th})}, \quad (41)$$

or equivalently, in terms of the original parameters

$$I_{pc} = \frac{(\mu_1 - \mu_{1th})^2}{2(b_{21}\mu_{2s} - b_1\mu_{1th})}. \quad (42)$$

We note that a positive value of I_{pc} requires the inequality

$$b_2\mu_{2s} - b_1\mu_{1th} > 0 \quad (43)$$

which matches the condition for a subcritical steady bifurcation (7) only if $b_2 = b_1$. If $b_2 \neq b_1$, the inequality (43) depends on both b_1 and b_2 and is a necessary condition for excitability.

With Eq. (41), we may rewrite Eq. (40) as

$$I = I_p - I_{pc} + \frac{I_{pc}}{\alpha^2}(\alpha + x)^2. \quad (44)$$

If $I_p < I_{pc}$, the trajectory terminates at $I = 0$ and

$$x = -\alpha + \sqrt{\alpha^2 \frac{I_{pc} - I_p}{I_{pc}}}. \quad (45)$$

On the other hand if $I_p > I_{pc}$, the trajectory is parabolic with a minimum at $x = -\alpha$. Using Eqs. (44), (38), and the definition of I_{pc} given by Eq. (42), we obtain the following equation for $u = x + \alpha$:

$$u' = \frac{1}{2} \left(\alpha^2 \frac{I_p - I_{pc}}{I_{pc}} + u^2 \right), \quad u(0) = \alpha. \quad (46)$$

Equation (46) is the normal form equation for a saddle-node bifurcation and can be integrated. The onset of a successful intensity pulse occurs after a time delay. Dubbeldam *et al.* [6] defined this delay as the critical time when $I(T)$ has reached its minimal value before quickly increasing. The minimum of I occurs at $u = 0$ when $T = T_c$ defined as

$$T_c \equiv -\frac{2}{\alpha \sqrt{\frac{I_p - I_{pc}}{I_{pc}}}} \arctan \left(\frac{1}{\sqrt{\frac{I_p - I_{pc}}{I_{pc}}}} \right) \quad (\alpha < 0). \quad (47)$$

Using Eq. (28) for α and $t_c = T_c/\varepsilon$, we obtain

$$t_c = \frac{2}{(\mu_{1th} - \mu_1) \sqrt{\frac{I_p - I_{pc}}{I_{pc}}}} \arctan \left(\frac{1}{\sqrt{\frac{I_p - I_{pc}}{I_{pc}}}} \right). \quad (48)$$

The effect of $b_2 \neq b_1$ appears in Eq. (48) through I_{pc} . If $I_p - I_{pc} \rightarrow 0$, the arctan function approaches $\pi/2$ and t_c essentially follows an $(I_p - I_{pc})^{-1/2}$ scaling law typical of trajectories near a saddle node bifurcation point (see [26], p. 100). On the other hand, t_c is inversely proportional to $\mu_{1th} - \mu_1$. This is consistent with the critical slowing down as we approach the transcritical steady bifurcation point $\mu_1 = \mu_{1th}$.

B. Incoherent perturbation

We next consider the case of an incoherent perturbation defined by the initial conditions (10). Figure 6 illustrates the emergence of an excitable pulse for different perturbations G_p . By contrast to the case of a coherent perturbation, we note in Fig. 6(a) that the maximum of the intensity pulse increases with G_p which is in agreement with the analysis in Sec. II. Figure 6(b) shows two numerical trajectories starting from below and above the critical perturbation $G_p = G_{pc}$ ($2.98 < G_{pc} < 2.99$). Using the parameters listed in Eq. (4), $\mu_1 = 2.9$ and $I_0 = 10^{-2}$, we evaluate the analytical approximation (53) derived below and obtain $G_{pc} \simeq 2.97$ which is close to the numerical estimate.

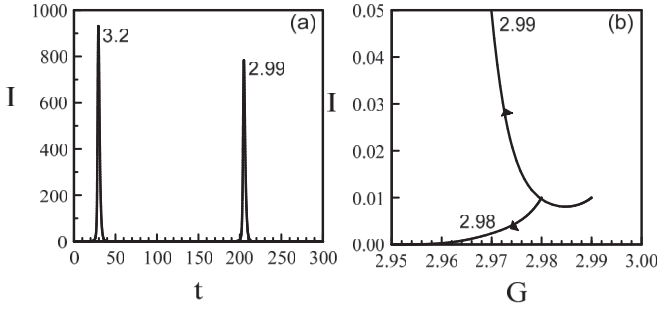


FIG. 6. Excitable pulses initiated by an incoherent perturbation. (a) Two intensity pulses were initiated by a perturbation G_p close and far from the critical perturbation. (b) Low intensity phase-plane (G, I) showing trajectories resulting from a below ($G_p = 2.98$) and an above critical perturbation ($G_p = 2.99$). The values of the parameters are listed in Eq. (4), $\mu_1 = 2.9$, and $I(0) = I_0 = 10^{-2}$.

The analysis of the laser equations in the limit $b_{1,2} \rightarrow 0$ is similar to the one detailed in the previous subsection. Instead of Eq. (39), the initial conditions for I and x now are

$$I(0) = I_0 \ll 1 \quad \text{and} \quad x(0) = g_p = \frac{G_p - \mu_{1th}}{\varepsilon} = O(1). \quad (49)$$

A first integration of Eqs. (37) and (38) leads to the trajectory

$$I = I_0 + \frac{1}{2(b_{21}\mu_{2s} - \mu_{1th})}((\alpha + x)^2 - (\alpha + g_p)^2). \quad (50)$$

The critical initial condition $g_p = g_{pc}$ corresponds to the trajectory leading to the saddle $(I, x) = (0, -\alpha)$. Using Eq. (50), we find that

$$g_{pc} = -\alpha - \sqrt{2(b_{21}\mu_{2s} - \mu_{1th})I_0}. \quad (51)$$

The condition for a successful excitable pulse now is

$$g_p > g_{pc}. \quad (52)$$

In terms of the original parameters, Eq. (51) takes the form

$$G_{pc} = \mu_{1th} - \sqrt{2(b_2\mu_{2s} - b_1\mu_{1th})I_0}. \quad (53)$$

Using Eq. (51), we may rewrite Eq. (50) as

$$I = I_0 + \frac{I_0}{(g_{pc} + \alpha)^2}((\alpha + x)^2 - (\alpha + g_p)^2). \quad (54)$$

Using then Eqs. (54), (38), and the definition of g_{pc} given by Eq. (51), the equation for $u = x + \alpha$ takes the form

$$u' = \frac{1}{2}((g_{pc} + \alpha)^2 - (g_p + \alpha)^2 + u^2), \quad u(0) = g_p + \alpha. \quad (55)$$

This equation can be integrated. The onset of an intensity pulse appears after a delay. However, we need to be careful about its definition. If we define the delay as the time for which the intensity reaches its minimum as in the previous subsection and as illustrated in Fig. 6(b) for $G_p = 2.99$, the initial perturbation g_p needs to satisfy the inequalities

$$g_{pc} < g_p \leq -\alpha. \quad (56)$$

See Fig. 7. If $g_p > -\alpha$, the intensity increases monotonically but without exhibiting a minimum. From the solution, we find

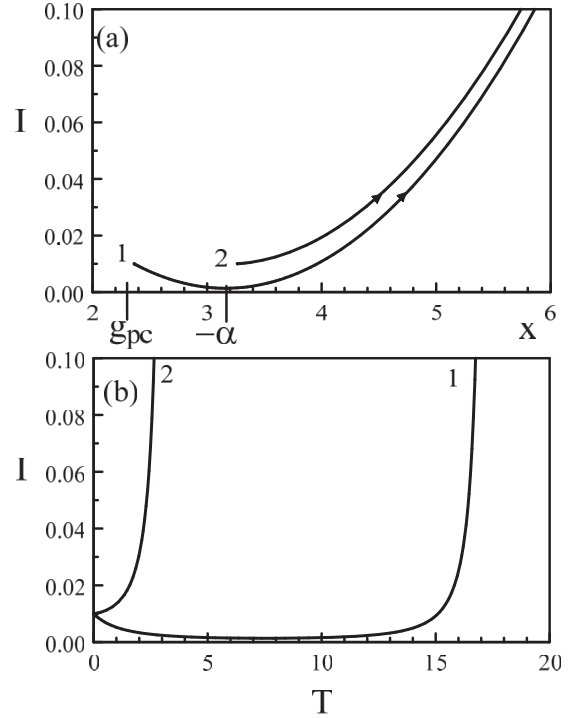


FIG. 7. Two trajectories in the phase plane (x, I) (a) and their associated time traces $I = I(T)$ (b). Parameters are listed in Eq. (4), $\mu_1 = 2.9$, and $I(0) = I_0 = 10^{-2}$. The two trajectories are starting from initial conditions where (1) $x(0) < -\alpha$ and (2) $x(0) > -\alpha$, respectively.

that the minimum of the intensity appears at

$$T_c = \frac{2}{\sqrt{(g_{pc} + \alpha)^2 - (g_p + \alpha)^2}} \times \arctan\left(\frac{-(g_p + \alpha)}{\sqrt{(g_{pc} + \alpha)^2 - (g_p + \alpha)^2}}\right). \quad (57)$$

In terms of the original parameters, Eq. (57) implies that $t_c = T_c/\varepsilon$ is given by

$$t_c = \frac{2}{\sqrt{F}} \arctan\left(\frac{-(G_p - \mu_{1th} + \mu_1 - \mu_{1th})}{\sqrt{F}}\right), \quad (58)$$

where G_{pc} is defined by Eq. (53) and

$$F \equiv (G_{pc} - \mu_{1th} + \mu_1 - \mu_{1th})^2 - (G_p - \mu_{1th} + \mu_1 - \mu_{1th})^2. \quad (59)$$

If $G_p \rightarrow G_{pc}^+$, $F \sim G_p - G_{pc}$ and $t_c \rightarrow \infty$ as the inverse of the square root of $G_p - G_{pc}$. This scaling law is again typical of a solution near a saddle.

V. DISCUSSION

Based on single fiber recordings, Hodgkin [4] identified different classes of excitability. Type I excitability is characterized by an ‘all-or-nothing’ behavior consisting either of a significant pulse (that is, an action potential) or a simple decay back to rest. If the action potential occurs, it has always roughly the same amplitude. Mathematically, spike generation

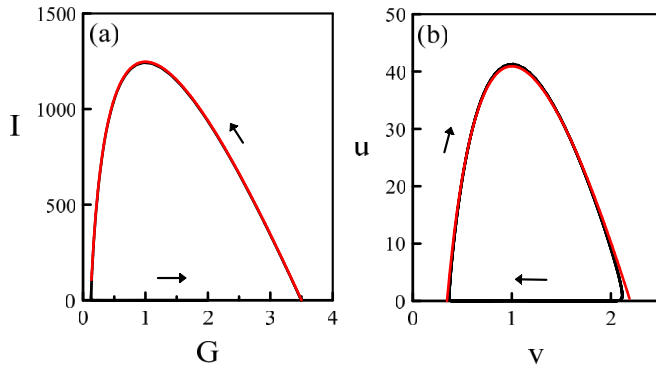


FIG. 8. Large pulses in phase-plane. (a) Excitable pulse solution of Eqs. (11) and (12). $\mu_2 = 2$, $s = 10$, $b_1 = 10^{-3}$, $\mu_1 = 2$, $G(0) = 3.5$. The approximation (21) is the red parabola that perfectly match the numerical solution. (b) Closed orbit of the Lotka-Volterra equations. $\varepsilon = 10^{-2}$, $u(0) = 10^{-3}$, and $v(0) = 2$. The red parabola is given by Eq. (64) with $v_0 = 0.345$.

is essentially a two-dimensional phenomenon of the van der Pol type involving fast activation to produce the rapid upstroke and slower recovery to produce the subsequent downstroke. The LSA exhibits the properties of a Type I excitable system and an initial perturbation of the intensity above threshold indeed leads to the expected behavior. However, if the initial perturbation is on the gain, the amplitude of the laser spike significantly depends on the amplitude of the initial perturbation. By analyzing the two variable LSA equations in Sec. III, we found that the fast dynamics is described by Eqs. (19) and (20), in first approximation. These equations are not of the van der Pol type because they admit a one-parameter family of orbits in phase-plane. Instead, the slow-fast dynamics of the LSA is

of Lotka-Volterra (LV) type as we shall now demonstrate. In dimensionless form, the LV equations are given by [27]

$$u' = u(1 - v), \quad (60)$$

$$v' = \varepsilon v(u - 1), \quad (61)$$

where ε is the only parameter. If $\varepsilon \rightarrow 0$, $u = O(\varepsilon^{-1})$ and $v = O(1)$, a large part of the orbit in phase-plane is well described by the reduced equations [28]

$$u' = u(1 - v), \quad (62)$$

$$v' = \varepsilon v u \quad (63)$$

which are equivalent to Eqs. (19) and (20). With the initial conditions $u = u_0 = 0$ and $v = v_0 < 1$, trajectories in terms of $u = u(v)$ are given by

$$u = \varepsilon^{-1} [\ln(v/v_0) - (v - v_0)]. \quad (64)$$

Figure 8 illustrates the similitude of the LSA and LV responses.

In conclusion we have investigated the emergence of excitable spikes in microlasers with integrated saturable absorber. Our results clarify the dynamical differences between coherent and incoherent perturbations and emphasize particular features of the slow-fast response of the LSA.

ACKNOWLEDGMENTS

T.E. acknowledges the support of the Fonds de la Recherche Scientifique (FNRS) (Belgium). This work benefited from the support of the Belgian Science Policy Office under Grant No. IAP-7/35 “photonics@be.” S.B. acknowledges partial support from ANR Optiroc and from the French Renatech Network.

- [1] J. Keener and J. Sneyd, *Mathematical Physiology I Cellular Physiology*, Interdisciplinary Applied Mathematics, 2nd ed. (Springer, Berlin, 2009).
- [2] *Computational Cell Biology*, Interdisciplinary Applied Mathematics Vol. 20, edited by C. P. Fall, E. S. Marland, J. M. Wagner, and J. J. Tyson (Springer, Berlin, 2002).
- [3] G. B. Ermentrout and D. H. Terman, *Mathematical Foundations of Neuroscience*, Interdisciplinary Applied Mathematics Vol. 35 (Springer, Berlin, 2010).
- [4] A. L. Hodgkin, The local electric changes associated with repetitive action in a non-medullated axon, *J. Physiol.* **107**, 165 (1948).
- [5] W. Lu, D. Yu, and R. G. Harrison, Excitability in a nonlinear cavity, *Phys. Rev. A* **58**, R809 (1998).
- [6] J. L. A. Dubbeldam, B. Krauskopf, and D. Lenstra, Excitability and coherence resonance with saturable absorber, *Phys. Rev. E* **60**, 6580 (1999).
- [7] J. L. A. Dubbeldam and B. Krauskopf, Self-pulsations of lasers with saturable absorber: dynamics and bifurcations, *Opt. Commun.* **159**, 325 (1999).
- [8] F. Plaza, M. G. Velarde, F. T. Arecchi, S. Boccaletti, M. Ciofini, and R. Meucci, Excitability following an avalanche-collapse process, *Europhys. Lett.* **38**, 85 (1997).
- [9] M. A. Larotonda, A. Hnilo, J. M. Mendez, and A. M. Yacomotti, Experimental investigation on excitability in a laser with saturable absorber, *Phys. Rev. A* **65**, 033812 (2002).
- [10] S. Barbay, R. Kuszelewicz, and A. Giacomotti, Excitability in a semiconductor laser with saturable absorber, *Opt. Lett.* **36**, 4476 (2011).
- [11] A. M. Yacomotti, M. C. Eguia, J. Aliaga, O. E. Martinez, G. B. Mindlin, and A. Lipsich, Interspike Time Distribution in Noise Driven Excitable Systems, *Phys. Rev. Lett.* **83**, 292 (1999).
- [12] M. Giudici, C. Green, G. Giacomelli, U. Nespolo, and J. R. Tredicce, Andronov bifurcation and excitability in semiconductor lasers with optical feedback, *Phys. Rev. E* **55**, 6414 (1997).
- [13] J. R. Tredicce, Excitability in laser systems: The experimental side, in *Fundamental Issues of Nonlinear Laser Dynamics*, edited by B. Krauskopf and D. Lenstra, AIP Conf. Proc. No. 548 (AIP, Melville, NY, 2000), p. 238.
- [14] H. J. Wünsche, O. Brox, M. Radziunas, and F. Henneberger, Excitability of a Semiconductor Laser by a Two-Mode Homoclinic Bifurcation, *Phys. Rev. Lett.* **88**, 023901 (2001).
- [15] M. Turconi, B. Garbin, M. Feyereisen, M. Giudici, and S. Barland, Control of excitable pulses in an injection-locked semiconductor laser, *Phys. Rev. E* **88**, 022923 (2013).

- [16] B. Garbin, A. Dolcemascolo, F. Prati, J. Javaloyes, G. Tissoni, and S. Barland, Refractory period of an excitable semiconductor laser with optical injection, *Phys. Rev. E* **95**, 012214 (2017).
- [17] B. Romeira, R. Avó, J. M. L. Figueiredo, S. Barland, and J. Javaloyes, Regenerative memory in time delayed neuromorphic photonic resonators, *Sci. Rep.* **6**, 19510 (2016).
- [18] J. Robertson, T. Deng, J. Javaloyes, and A. Hurtado, Controlled inhibition of spiking dynamics in VCSELs for neuromorphic photonics: Theory and experiments, *Opt. Lett.* **42**, 1560 (2017).
- [19] P. R. Prucnal and B. J. Shastri, *Neuromorphic Photonics* (CRC Press/Taylor & Francis Group, New York, 2017).
- [20] Q. Li, Z. Wang, C. Cui, R. Li, Y. Li, B. Liu, and C. Wu, Simulating the spiking response of VCSEL-based optical spiking neuron, *Opt. Commun.* **407**, 327 (2018).
- [21] B. Romeira, J. Javaloyes, C. N. Ironside, J. M. L. Figueiredo, S. Balle, and O. Piro, Excitability and optical pulse generation in semiconductor lasers driven by resonant tunneling diode photo-detectors, *Opt. Exp.* **21**, 20931 (2013).
- [22] F. Selmi, R. Braive, G. Beaudoin, I. Sagnes, R. Kuszelewicz, and S. Barbay, Relative Refractory Period in an Excitable Semiconductor Laser, *Phys. Rev. Lett.* **112**, 183902 (2014).
- [23] F. Selmi, R. Braive, G. Beaudoin, I. Sagnes, R. Kuszelewicz, T. Erneux, and S. Barbay, Spike latency and response properties of an excitable micropillar laser, *Phys. Rev. E* **94**, 042219 (2016).
- [24] M. Bache, F. Prati, G. Tissoni, R. Kheradmand, L. Lugiato, I. Protzenko, and M. Brambilla, Cavity soliton laser based on VCSEL with saturable absorber, *Appl. Phys. B* **81**, 913 (2005).
- [25] T. Erneux and P. Glorieux, *Laser Dynamics* (Cambridge University Press, Cambridge, 2010).
- [26] S. H. Strogatz, *Nonlinear Dynamics And Chaos: With Applications To Physics, Biology, Chemistry, And Engineering (Studies in Nonlinearity)*, 1st ed. (Westview Press, Boulder, CO, 2001), p. 99.
- [27] J. D. Murray, *Mathematical Biology I: An Introduction*, Interdisciplinary Applied Mathematics, 3rd ed., Vol. 17 (Springer, Berlin, 2002).
- [28] J. Grasman, *Asymptotic Methods of Relaxation Oscillations and Applications*, Applied Mathematical Sciences Vol. 63 (Springer, New York, 1987).